RPE | Radiation Physics & Engineering
A Peer-Reviewed Journal
Published by K.N. Toosi University of Technology
http://rpe.kntu.ac.ir
Research Article

Radiation Physics and Engineering 2026; ?(?):?–?

Design of neutron beam for neutron radiography base on the use of TRR thermal column

Saeed Sabouri[a], Yaser Kasesaz[b,*], Mohsen Kheradmand Saadi[a]

[a] *Department of Nuclear Engineering, SR.C, Islamic Azad University, Tehran, Iran*
[b] *Nuclear Science and Technology Research Institute, Tehran, Iran*

HIGHLIGHTS

- 144 configurations have been investigated using MCNPX, varying gamma shield material to maximize beam purity.
- Bismuth significantly outperforms Lead as a gamma shield due to its lower neutron absorption cross-section.
- The optimized design achieves a thermal neutron flux of 1.0×10^6 n.cm^{-2}.s^{-1} at $L/D = 114$ under full-core conditions.

ABSTRACT

In this study, a thermal neutron beam suitable for neutron radiography (NR) was designed based on the thermal column of the Tehran Research Reactor (TRR). The existing air-filled channel inside the graphite thermal column was utilized to implement a dedicated beamline consisting of a gamma filter slab, a boron carbide thermal neutron absorber with a central aperture, and a conical collimator. A comprehensive parametric optimization was performed using the MCNPX Monte Carlo code. A total of 144 configurations were evaluated by varying the gamma filter material, aperture thickness, aperture radius and the distance between the aperture and image position. Bismuth demonstrated superior performance compared with lead due to its lower neutron absorption and effective gamma attenuation. The optimized configuration, employing 5 cm of Bi filter and a 5 cm B_4C aperture with a 2 cm radius, achieved a thermal neutron flux of 1.0×10^6 n.cm^{-2}.s^{-1} at $L/D = 114$ under full-core simulation conditions at reactor full power. The neutron-to-gamma ratio and fast neutron suppression were significantly improved, while the gamma dose rate was substantially reduced compared with the existing E-beam tube NR facility at TRR. A secondary surface-source methodology was implemented to accelerate the parametric study and was subsequently validated against full-core simulations. Although the simplified model overestimated absolute flux values, it accurately reproduced relative performance trends, confirming its suitability for design optimization. The results demonstrate that the TRR thermal column can provide an efficient and high-quality neutron beam for advanced NR applications with enhanced beam purity and radiation safety.

KEYWORDS

Neutron Radiography
Tehran Research Reactor
Thermal column
MCNPX Monte Carlo code

HISTORY

Received:
Revised:
Accepted:
Published:

1 Introduction

Neutron Radiography (NR) is a non-destructive testing technique that utilizes neutrons to image the internal structure of materials (Mühlbauer et al., 2005). Unlike traditional X-ray radiography, which uses X-rays, neutron radiography relies on the interaction between neutrons and atomic nuclei, offering unique advantages for certain applications. This method is particularly useful for materials that are transparent to X-rays but opaque to neutrons, such as light elements like hydrogen, lithium, and boron (Tawalare, 2022; Hashimoto, 2022)s. A major advantage of NR over X-ray imaging is its sensitivity to light elements, particularly hydrogen, which is essential for imaging objects containing water, polymers, and certain composites. This makes NR an invaluable tool in diverse fields, including aerospace, nuclear industries, and even archaeology (Nallaperumal et al., 2022; Lehmann, 2009; Aswal et al., 2022). NR also is widely applied for inspecting materials such as aircraft parts, composite materials, fuel elements, and cultural heritage artifacts (Lehmann, 2009; Dastjerdi et al., 2016b).

*Corresponding author: YKasesaz@aeoi.org.ir

https://doi.org/

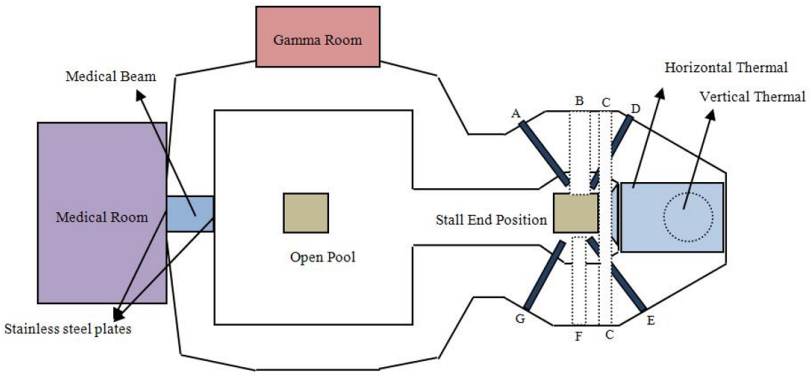

Figure 1: A schematic view of TRR and its irradiation facilities (Dastjerdi and Khalafi, 2015).

While NR is highly effective, it requires access to a neutron source, typically provided by nuclear reactors or particle accelerators (Mokhtari and Dastjerdi, 2023; Joseph et al., 2025). Specialized facilities, such as research reactors and synchrotron radiation sources, provide the necessary infrastructure to generate neutrons with adequate intensity and energy levels to perform high-quality imaging.

In addition to conventional neutron radiography, advanced techniques such as neutron tomography and neutron diffraction radiography are also being explored, offering three-dimensional imaging capabilities and detailed material phase analysis, respectively. These techniques allow for more comprehensive studies of complex materials and structures, expanding the potential applications of neutron imaging.

One of the key challenges in this method is the design of the neutron beam, as its characteristics significantly influence the quality of radiographic images. The neutron beam must have properties such as appropriate intensity, uniformity, and high accuracy in order to provide high-quality images with sufficient resolution. The recommended value of neutron beam parameter for NR is presented in Table 1 (Dastjerdi et al., 2016a; Roy, 2022).

In NR, image quality strongly depends on proper neutron beam design, as transmitted neutrons through different materials form the final radiographic image. A well-designed beam enhances accuracy, uniformity, and resolution, which is particularly important for complex and multilayered materials with varying densities and compositions. Precise control of beam size and intensity enables the detection of fine defects such as cracks and voids in advanced engineering components, including composites and aerospace structures. Moreover, due to the high sensitivity of neutrons to light elements such as hydrogen and boron, optimized beam characteristics are essential for applications involving biological materials and nuclear fuels, where neutron-based imaging provides unique internal structural information.

Tehran Research Reactor (TRR) is a 5 MW pool-type research reactor primarily used for scientific research, educational purposes, and medical isotope production. It is one of the oldest and most significant research reactors in the Middle East and has played a pivotal role in advancing nuclear science and technology in Iran. The TRR operates under a thermal neutron flux of up to 10^{13} n.cm^{-2}.s^{-1}, which makes it suitable for a wide range of neutron-based experiments. Its fuel was converted from HEU to LEU in 1987 and now, the reactor operates with domestic nuclear fuel. TRR has several irradiation facilities that support a variety of neutron and gamma applications, including radioisotope production (Vosoughi et al., 2023; Bagheri et al., 2015; Forughi et al., 2013), neutron diffractometry (Bavarnegin et al., 2025), and Neutron Radiography (Dastjerdi et al., 2016a; Dastjerdi and Khalafi, 2015). Figure 1 shows a schematic view of TRR and its irradiation facilities (Kasesaz et al., 2016).

As shown in Fig. 1, TRR is equipped with a thermal column. The thermal column is a horizontal channel with a cross-section of 1.5×1.5 m^2 and a length of approximately 3 m. It is completely filled with graphite blocks arranged in different configurations, as illustrated in Fig. 2 (Kasesaz et al., 2014). In 2014, the arrangement and configuration of the graphite blocks were modified so that two rows of the central graphite blocks could be removed, creating an air-filled channel with dimensions of $30 \times 30 \times 240$ cm, as shown in Fig. 3. The purpose of this modification was to generate a thermal neutron beam for neutron therapy research (Kasesaz et al., 2014). The thermal neutron flux at the beginning of this channel is approximately 10^{11} n.cm^{-2}.s^{-1} (Kasesaz et al., 2014).

TRR also has an active NR facility based on an E-beam tube (Fig. 4). The thermal neutron flux in this facility is 6.5×10^6 n.cm^{-2}.s^{-1} (Dastjerdi et al., 2016a), and the field of view is approximately 15 cm, which is suitable for neutron imaging applications.

In the present study, a new neutron beam has been designed based on the TRR thermal column. For this purpose, the MCNPX Monte Carlo code was used (Waters and Laboratory, 2002). The design goal is to achieve a neutron beam with the parameters presented in Table 1 (Roy, 2022).

Table 1: Recommended value of neutron beam parameter for NR (Dastjerdi et al., 2016a; Roy, 2022)

Parameter	Desired value
φ_{th} ($\times 10^6$ n.cm^{-2}.s^{-1})	>1
n/γ ($\times 10^5$ n.cm^{-2}.mrem^{-1})	>1
L/D	>100

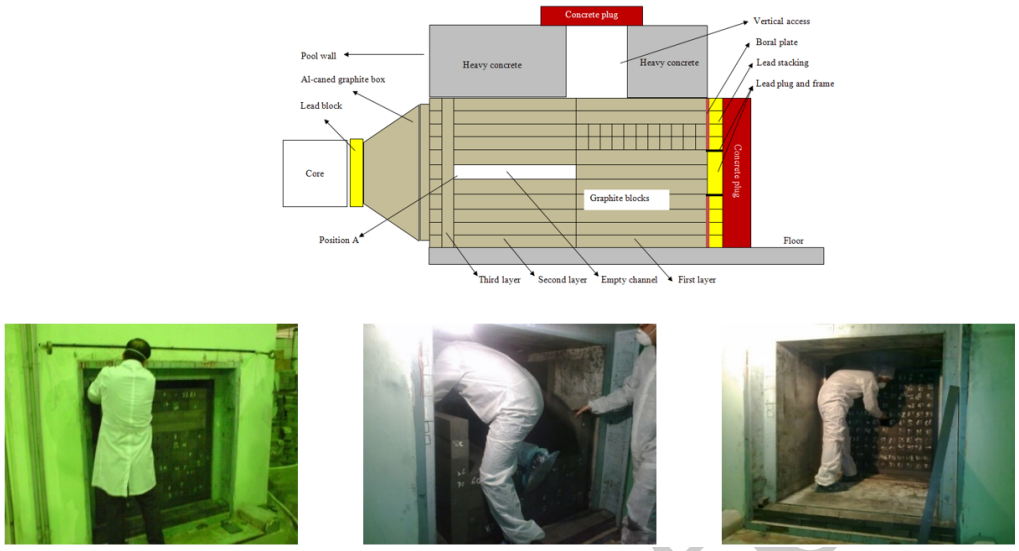

Figure 2: The structure of TRR thermal column (Kasesaz et al., 2016).

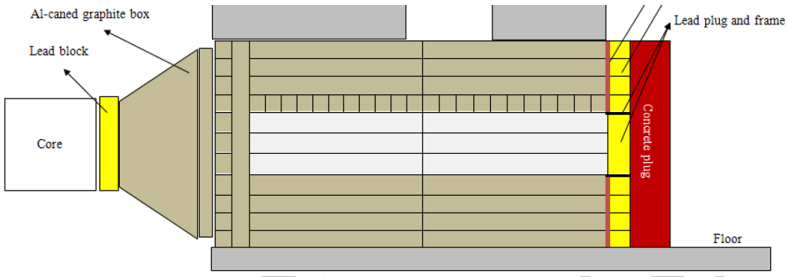

Figure 3: The air-filled channel created after removing 18 graphite blocks (Kasesaz et al., 2016).

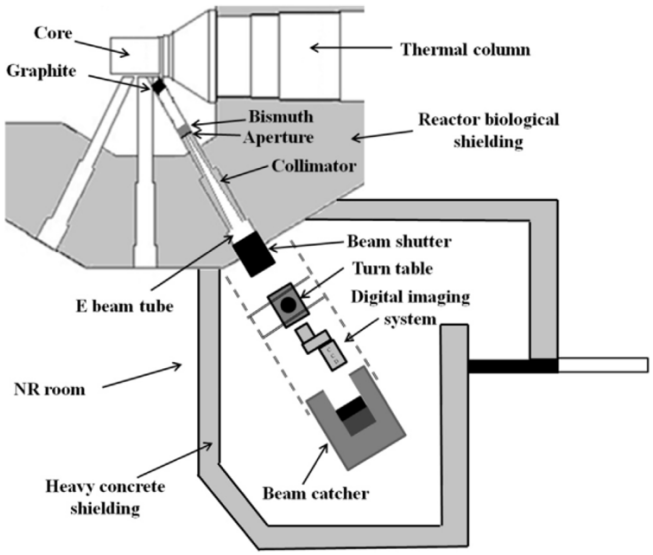

Figure 4: A schematic of NR facility at TRR based on E-beam tube (Dastjerdi et al., 2016a).

2 Materials and Methods

2.1 TRR simulation

In the first stage of this study, TRR was modeled in comprehensive geometrical and material detail. Particular emphasis was placed on the reactor thermal column, given its critical role in moderating and guiding neutron flux for beam applications. The developed three-dimensional model incorporated all relevant structural components, including graphite moderator regions and the central air column. The latter serves as the designated location for the installation of the designed collimator system for different applications in the future. A schematic representation of the modeled geometry is presented in Fig. 5.

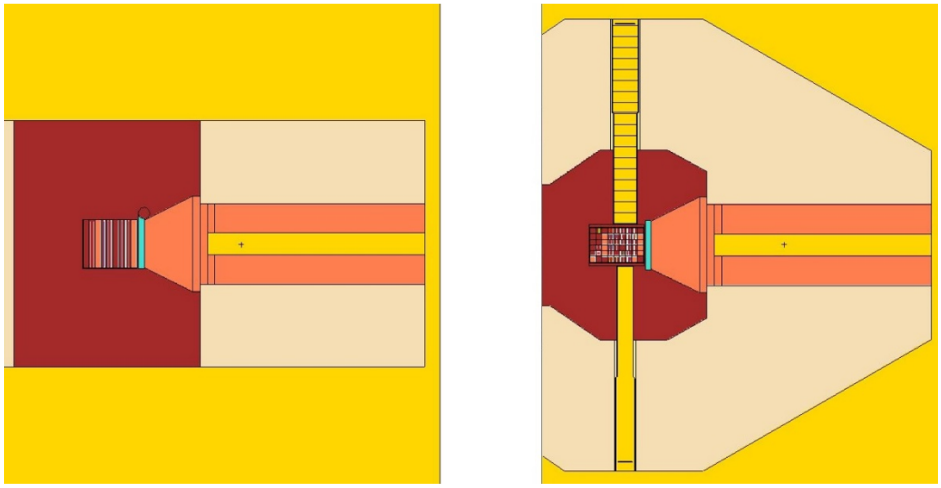

Figure 5: The simuated model of TRR includign the reactor core, pool, beam tubes and the thermal coilmn (Left: side view, Right: top view).

2.2 Modeling of the neutron and gamma source

Due to the large geometric dimensions and complexity of the simulated configuration, achieving statistically reliable results (relative error below 10%) required substantial computational time. Considering that approximately 200 different collimator configurations were investigated in this work, direct simulation of the full reactor core for each case would have been computationally inefficient. To address this limitation, a two-step surface source methodology was adopted. First, the neutron and gamma energy spectra were calculated on a surface positioned at the entrance of the thermal column. In the subsequent stage, the reactor core was removed from the computational model, and the previously defined surface was employed as an equivalent neutrongamma source. This approach significantly reduced computational time while preserving the spectral and spatial characteristics of the radiation field entering the thermal column.

For improved spatial accuracy, the source surface was subdivided into 11 concentric circular regions. The multigroup neutron and gamma spectra were calculated independently for each region in order to account for radial variations in flux intensity and energy distribution. These calculations were performed using the MCNP F1:n and F11:p tally cards in combination with the FSn and En energy bin definition cards. The defined regions are illustrated in Fig. 6, and the resulting neutron and gamma spectral data are summarized in Tables 2 and 3, respectively.

Based on the obtained spectral distributions, a new composite neutrongamma source was defined at the same location. The source was implemented in MCNP using the ERG=D1, PAR=FERG=D2, and RAD=FERG=D3 cards, enabling explicit specification of energy distribution, particle type, and radial dependence according to the calculated multi-group data. This procedure ensured that the simplified model accurately reproduced the radiation characteristics of the original full-core simulation while substantially improving computational efficiency.

2.3 Neutron beam design

In the next step, the detailed configuration of the neutron beamline was modeled and analyzed. The beamline consists of several principal components designed to shape the neutron spectrum, attenuate gamma radiation, and achieve suitable collimation for NR applications. The main structural elements of the beamline include:

1. A gamma filter slab
2. A thermal neutron absorber slab incorporating a central cylindrical aperture
3. A collimator

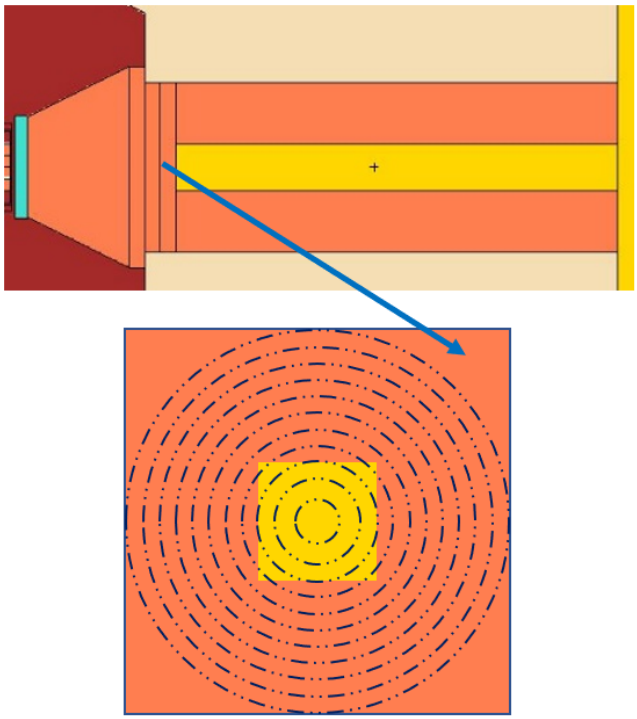

Figure 6: A view of the MCNP model of the thermal column and defined regions for secondary neutron and gamma source.

Table 2: Neutron intensity in different group of energy in 11 defined regions.

Region No.	0-0.6 eV ($\times 10^{14}$ s^{-1})	0.6 eV-0.01 MeV ($\times 10^{11}$ s^{-1})	0.01-20 MeV ($\times 10^{10}$ s^{-1})	Total ($\times 10^{14}$ s^{-1})
1	0.18	0.25	0.44	0.18
2	0.53	0.73	1.48	0.53
3	0.86	1.01	2.31	0.87
4	1.16	1.15	2.54	1.16
5	1.40	1.22	2.89	1.40
6	1.58	1.26	3.57	1.58
7	1.69	1.30	4.91	1.69
8	1.71	1.34	5.69	1.71
9	1.65	1.19	4.58	1.65
10	1.51	0.84	4.23	1.51
11	2.56	1.12	5.24	2.57

Table 3: Gamma intensity in different group of energy in 11 defined regions.

Region No.	0-2 MeV ($\times 10^{13}$ s^{-1})	2-4 MeV ($\times 10^{12}$ s^{-1})	4-6 MeV MeV ($\times 10^{12}$ s^{-1})	6-8 MeV ($\times 10^{11}$ s^{-1})	Total ($\times 10^{13}$ s^{-1})
1	0.07	0.08	0.11	0.01	0.09
2	0.21	0.34	0.22	0.02	0.27
3	0.35	0.42	0.57	0.03	0.44
4	0.49	0.60	0.66	0.06	0.62
5	0.64	0.79	1.01	0.04	0.82
6	0.76	0.71	0.99	0.18	0.94
7	0.87	0.80	1.08	0.50	1.06
8	0.98	0.88	0.79	0.72	1.16
9	1.12	0.96	1.14	1.52	1.35
10	1.26	1.42	1.14	0.46	1.52
11	3.10	3.69	2.75	6.10	3.81

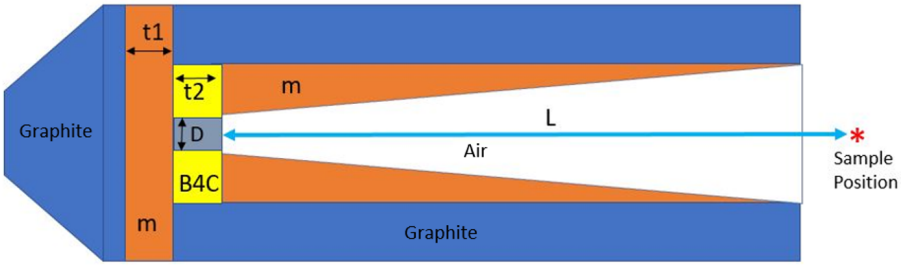

Figure 7: A schematic view of the neutron beam line structure: t_1 is the thickness of gamma filter slab, t_2 is the thermal neutron absorber thickness (B_4C), D (=2R) is the diameter of the hole and m is the gamma filter material (Bi or Pb).

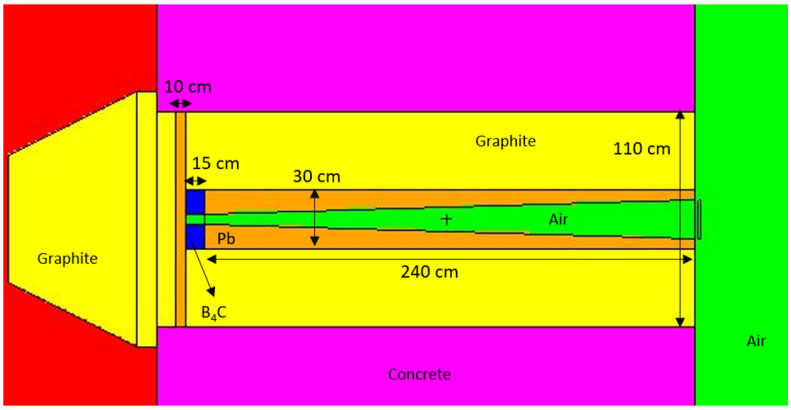

Figure 8: MCNP simulated geometry of the neutron beam line.

Figure 7 presents a schematic representation of the beamline layout, while Fig. 8 illustrates the detailed geometry implemented in the Monte Carlo simulation model.

As shown in Fig. 7, the gamma filter slab is positioned

Table 4: 10 cases with the highest thermal neutron flux for Pb material as the gamma filter.

Pb							
No.	t_1 (cm)	t_2 (cm)	R (cm)	φ_{th} ($\times 10^7$ n.cm^{-2}.s^{-1})	$\varphi_{th}/\varphi_{fast}$	n/γ ($\times 10^7$ n.cm^{-2}.mrem^{-1})	L/D
1	5	5	3	5.9	266	2.2	43
2	5	10	3	5.5	319	1.8	42
3	5	15	3	5.1	302	1.7	41
4	5	20	3	4.9	295	1.7	40
5	5	5	2.5	4.6	346	2.3	51
6	10	5	3	4.5	353	2.2	42
7	5	10	2.5	4.2	334	1.9	50
8	10	10	3	4.0	328	1.8	41
9	5	15	2.5	3.9	318	1.8	49
10	10	15	3	3.8	323	1.7	40

Table 5: 10 cases with the highest thermal neutron flux for Bi material as the gamma filter.

Bi							
No.	t_1 (cm)	t_2 (cm)	R (cm)	φ_{th} ($\times 10^7$ n.cm^{-2}.s^{-1})	$\varphi_{th}/\varphi_{fast}$	n/γ ($\times 10^7$ n.cm^{-2}.mrem^{-1})	L/D
1	5	5	3	14.5	806	5.0	43
2	10	5	3	13.4	850	5.4	42
3	5	5	2.5	12.4	934	5.4	51
4	5	10	3	12.3	718	4.0	42
5	15	5	3	12.1	993	5.7	41
6	10	10	3	11.2	747	4.5	41
7	5	15	3	11.1	658	3.6	41
8	10	5	2.5	11.0	985	5.7	50
9	5	5	2	10.7	1143	6.7	64
10	5	10	2.5	10.7	834	4.5	50

Table 6: The calculated thermal neutron flux ($\times 10^7$ n.cm^{-2}.s^{-1}) for different distances from the beam exit (different L) for 7 selected configuration (see Tables 4 and 5).

Bi-No.8		Bi-No.9		Bi-No.10		Bi-No.3		Bi-No.7		Bi-No.5	
L/D	φ_{th}	L/D	φ_{th}	L/D	φ_{th}	L/D	φ_{th}	L/D	φ_{th}	L/D	φ_{th}
50	11.1	64	10.5	50	10.4	51	12.6	50	4.2	51	4.6
60	3.9	77	3.7	60	4.0	61	4.6	60	2.4	61	2.6
70	2.5	89	2.4	70	2.5	71	2.9	70	1.7	71	1.8
80	1.7	102	1.6	80	1.8	81	2.1	80	1.2	81	1.3
90	1.3	114	1.2	90	1.4	91	1.5	90	0.9	91	1.0

upstream to attenuate the intense gamma radiation originating from the reactor core and surrounding structural materials. After of this layer, a thermal neutron absorber slab made of boron carbide (B_4C) is installed. This slab includes a central cylindrical hole that allows transmission of the useful neutron beam while suppressing scattered and off-axis neutrons. The conical structure serves as the primary neutron collimator. The annular region between the outer surface of the cone and the surrounding air channel is filled with gamma filter material to further reduce photon background and minimize radiation leakage. Two candidate materials were considered for this purpose: lead (Pb) and bismuth (Bi). These high-Z materials were selected due to their effective gamma attenuation properties and relatively low neutron absorption compared to other dense metals. The geometrical parameters of the conical collimator are defined as follows:

- The small radius of the cone is equal to the radius of the central aperture in the thermal neutron absorber slab (R).
- The large radius of the cone is fixed at 10 cm, corresponding to the desired beam diameter at the imaging plane.
- The total length of the cone is determined by the combined thicknesses of the gamma filter slab (t_1) and the thermal neutron absorber slab (t_2).

In order to obtain a neutron beam suitable for NR, several design parameters were systematically optimized. The primary variables considered in this study include t_1, t_2, R and m.

Boron carbide (B_4C) was selected as the thermal neutron absorber material due to its high neutron absorption cross-section for thermal neutrons and its effectiveness in suppressing unwanted scattered components while maintaining acceptable beam quality. For each combination of t_1, t_2, R, and filter material, the following performance indicators were calculated:

- Thermal neutron flux at the imaging plane
- Gamma dose rate
- L/D ratio (collimation ratio)

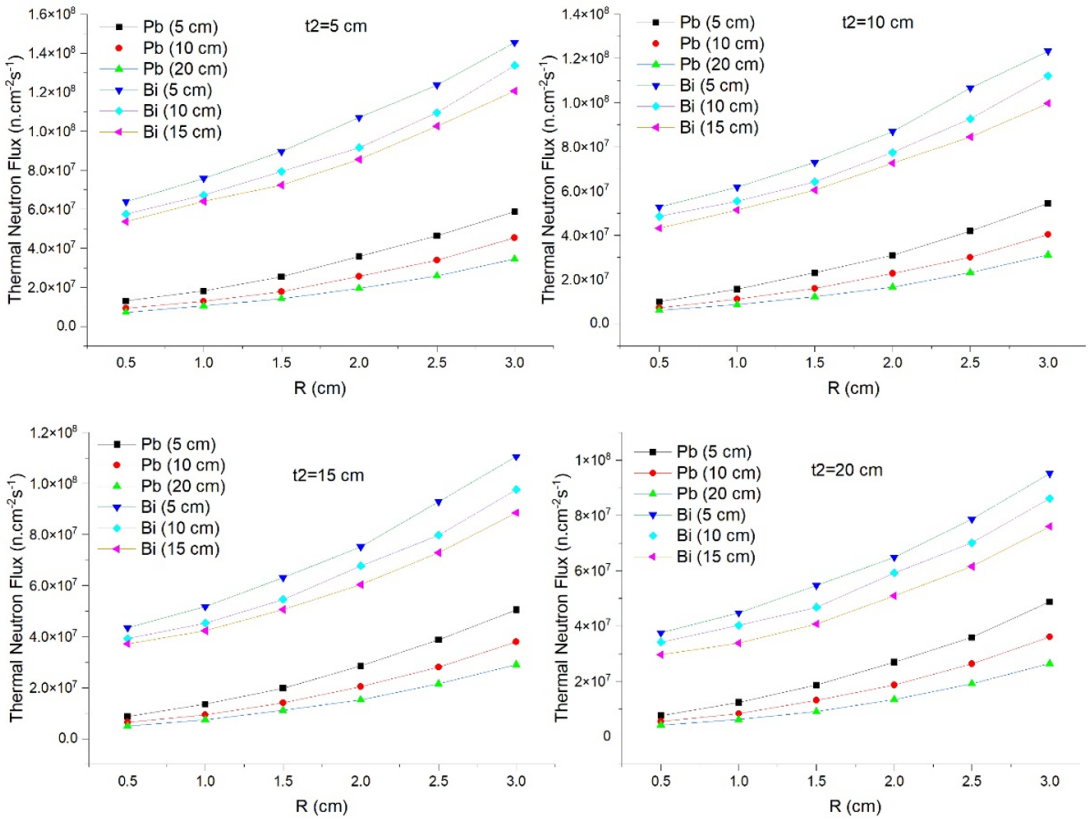

Figure 9: The calculated thermal neutron fluxes corresponding to different configurations.

MCNP F5:n/E5 cards have been used for thermal neutron flux calculation and F15:p/DE15/DF15 cards for gamma dose rate calculations. The L/D ratio, defined as the ratio of collimator length (L) to aperture diameter (D), is a key parameter governing spatial resolution in NR. Increasing L/D generally improves image sharpness but reduces neutron intensity; therefore, a trade-off analysis was necessary.

By considering multiple discrete values for each variable, a total of 144 different beamline configurations were simulated. This comprehensive parametric study allowed identification of optimal configurations that provide a high thermal neutron flux, reduced gamma contamination, and an appropriate L/D ratio for radiographic applications

3 Results and discussion

The neutron beam performance was evaluated for 144 different configurations obtained by varying the gamma filter thickness (t_1), thermal neutron absorber thickness (t_2), aperture radius (R), and filter material (Pb or Bi). The calculated thermal neutron fluxes corresponding to all configurations are presented in Fig. 9. A significant difference is observed between lead and bismuth as gamma filter materials. The configurations employing bismuth exhibit thermal neutron flux values approximately one order of magnitude higher than those using lead. This improvement can be attributed to the lower neutron absorption cross-section of Bi compared with Pb, combined with its effective gamma attenuation capability. Consequently, Bi provides superior neutron transmission while maintaining acceptable gamma suppression.

Figures 10 and 11 presents the calculated n/γ ratio and th/fast ratio respectively. In addition to the enhanced thermal neutron flux (φ_{th}), the n/γ ratio and $\varphi_{th}/\varphi_{fast}$ ratio are also substantially higher in Bi-based configurations. These results indicate improved spectral purity and reduced fast neutron contamination, both of which are essential for NR.

The results clearly demonstrate that the thermal neutron flux strongly depends on the aperture radius (R), as well as the slab thicknesses t_1 and t_2. Increasing R generally leads to higher thermal neutron flux due to reduced geometrical restriction. However, this comes at the expense of decreasing L/D ratio and spatial resolution. Smaller R values improve beam collimation and increase L/D, but reduce neutron intensity.

Increasing t_1 enhances gamma attenuation but may also reduce neutron intensity due to additional neutron scattering and absorption. An optimal thickness must balance dose reduction and neutron transmission.

The B_4C aperture effectively suppresses scattered and off-axis neutrons. However, excessive thickness reduces useful thermal neutron intensity. The results indicate that moderate t_2 values provide the best compromise between beam purity and flux.

Among the 144 configurations, the 10 cases with the highest thermal neutron flux for Pb and Bi were identified (Tables 4 and 5). While most selected cases exhibit acceptable φ_{th}, n/γ, and $\varphi_{th}/\varphi_{fast}$ values for NR appli-

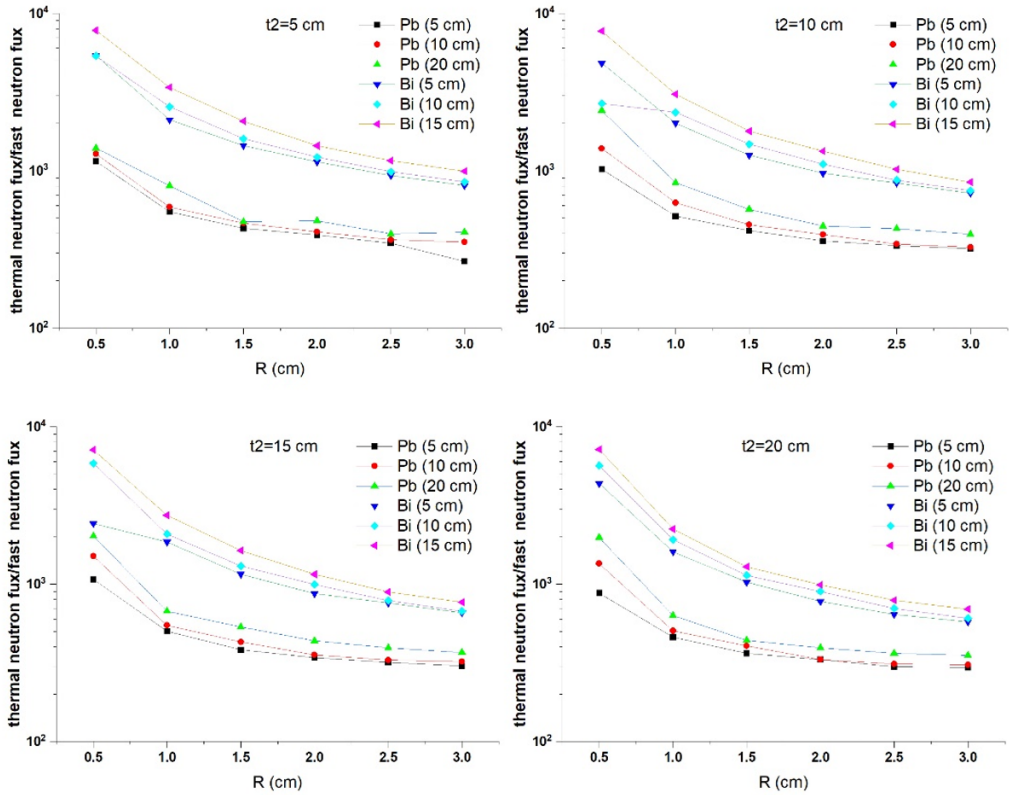

Figure 10: The calculated thermal to fast neutron fluxes ratio corresponding to different configurations.

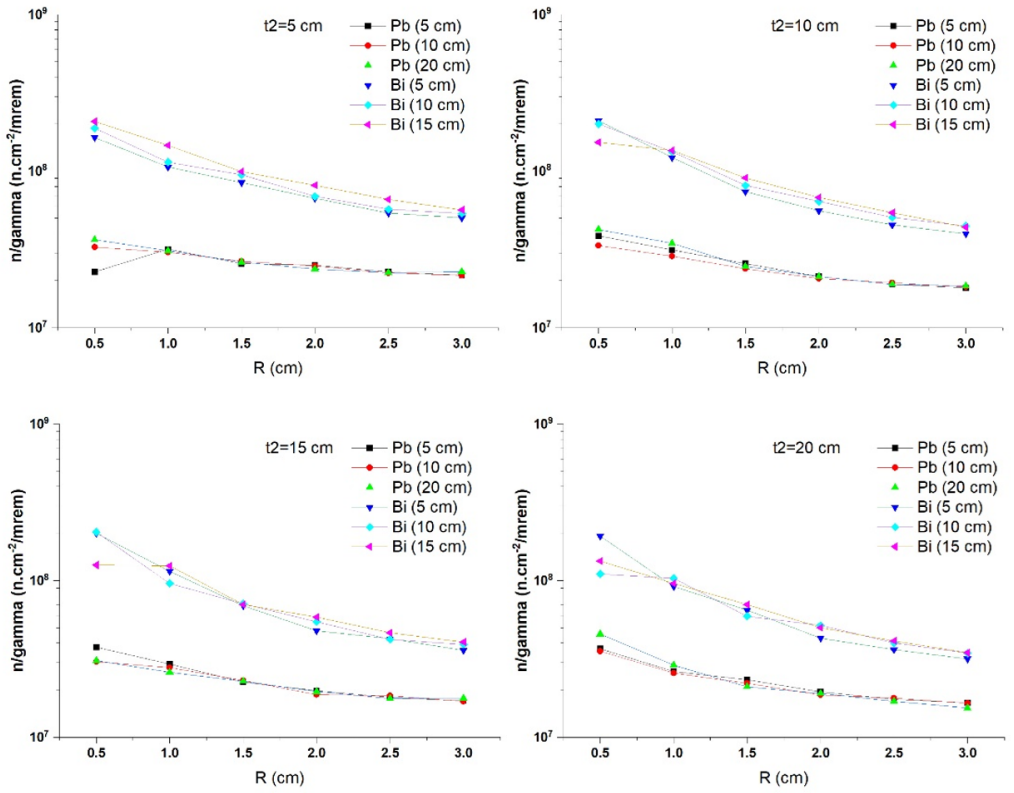

Figure 11: The calculated neutron flux to gamma dose rate ratio corresponding to different configurations.

cations, the L/D ratio required further optimization to reach values exceeding 100, which is typically desired for high-resolution imaging.

To achieve higher L/D values, configurations with L/D greater than 50 were selected for further analysis. For these cases, neutron beam parameters were recalcu-

Table 7: The final neutron beam parameters in comparison with the E-beam tube NR beam.

Parameter	-	E-beam tube	Thermal Column
φ_{th}	($\times 10^6$ n.cm^{-2}.s^{-1})	6.5	12.1
n/γ	($\times 10^5$ n.cm^{-2}.mren^{-1})	3.5	325
Gamma dose rate	(mrem)	18	0.4
L/D	-	150	114

Table 8: The calculated thermal neutron flux and gamma dose rate corresponding to real source and secondary source.

L/D	Thermal neutron flux ($\times 10^7$ n.cm^{-2}.s^{-1})		Gamma dose rate (mrem.s^{-1})	
	secondary source	real source	secondary source	real source
64	10.5	1.2	1.52	0.24
77	3.7	0.4	1.01	0.17
89	2.4	0.3	0.69	0.13
102	1.6	0.2	0.49	0.11
114	1.2	0.1	0.37	0.10

lated at different distances from the beam exit, effectively increasing the collimation length (L). The results are presented in Table 6.

As expected, increasing L/D results in a gradual decrease in thermal neutron flux due to geometrical beam divergence and attenuation. However, Bi-based configurations maintain significantly higher flux levels even at L/D values above 100. For instance, Bi-No.9 achieves $L/D = 114$ while maintaining acceptable neutron intensity, demonstrating the robustness of this configuration.

In the final step, the configuration providing the highest combined performance in terms of thermal neutron flux and L/D ratio was selected. The optimized beam parameters are summarized in Table 7 and compared with the existing neutron radiography system based on the E-beam tube configuration at the TRR.

Although the L/D of the E-beam tube is slightly higher, the optimized thermal column configuration provides nearly doubled thermal neutron flux, dramatically improved neutron-to-gamma ratio and significantly reduced gamma dose rate.

The large reduction in gamma dose (from 18 mrem to 0.4 mrem) represents a major improvement in beam quality and operational safety. Moreover, given the relatively high thermal neutron flux in the optimized configuration, it is reasonable to expect that further increases in L/D could be achieved without experiencing a prohibitive reduction in neutron intensity.

In the final step, in order to obtain more realistic and reliable neutron beam parameters, the optimized configuration was re-evaluated using the original full reactor input file, which includes the complete reactor core and all geometrical details of TRR. This step was performed to validate the accuracy of the previously defined secondary source method. In earlier stages of the study, a secondary neutron-gamma source was generated based on spectral calculations at the entrance of the thermal column. Although this approach significantly reduced computational time, it was necessary to compare its results with those obtained from a full-core simulation. For this purpose, neutron beam parameters were recalculated using the complete reactor core geometry, the full structural configuration and the selected beamline design. The results obtained from the secondary source simulation were directly compared with those derived from the full reactor simulation in order to assess the consistency and reliability of the simplified modeling approach. The calculated thermal neutron flux and gamma dose rate for both approaches are presented in Table 8 (based on the provided data).

The comparison clearly shows that the secondary source method consistently overestimates both thermal neutron flux and gamma dose rate relative to the full-core simulation. For example: in the first evaluation point, the thermal neutron flux obtained using the secondary source was 1.05×10^8 n.cm^{-2}.s^{-1}, while the corresponding value from the full simulation was 1.23×10^7 n.cm^{-2}.s^{-1}. Similarly, the gamma dose rate decreased from 1.52 mrem.s^{-1} (secondary source) to 0.236 mrem.s^{-1} (full simulation). This trend is observed consistently across all evaluation points. Despite the quantitative differences, an important observation is that the relative behavior of the beam parameters remains consistent between the two approaches; thermal neutron flux decreases progressively along the beamline and gamma dose rate follows the same attenuation trend. This consistency confirms that the secondary source approach correctly captures the overall physical behavior of the system, even though it overestimates absolute values. Although the secondary source method produces higher numerical values, it remains a valid and efficient tool for comparative design studies and parametric optimization. The key advantage of this method lies in its substantial reduction of computational time, especially when evaluating a large number of configurations. However, for final performance assessment and reporting of realistic beam parameters, the use of full-core simulation is essential.

The final results demonstrate that the optimized beamline configuration maintains acceptable neutron beam characteristics when evaluated under full reactor conditions. Gamma dose rates are significantly reduced in the complete model, which is favorable from a radiation protection standpoint. The optimized design remains suitable for neutron radiography applications even after applying realistic reactor modeling conditions.

4 Conclusions

This study demonstrates the MCNP feasibility of utilizing the thermal column of the Tehran Research Reactor as a high-performance neutron source for radiography applications. Through systematic Monte Carlo simulations performed with MCNPX, the effects of filter material, geometric parameters, and filter thickness were comprehensively evaluated. The results clearly indicate that bismuth is a superior gamma filter material compared with lead, providing significantly higher thermal neutron flux and improved neutron-to-gamma ratios while maintaining low gamma dose levels. The optimized beamline configuration achieved a thermal neutron flux of approximately 1.0106 ncms at $L/D = 114$ under realistic full-core conditions, meeting recommended criteria for neutron radiography. In comparison with the existing E-beam tube facility, the proposed design provides nearly doubled neutron flux, markedly improved spectral purity, and a substantial reduction in gamma dose rate.

The secondary surface-source approach proved to be an efficient tool for large-scale parametric optimization, although final performance assessment requires full-core reactor modeling to obtain realistic absolute values.

Overall, the proposed configuration offers a practical and effective pathway to upgrade neutron radiography capabilities at TRR. Future work should address detailed engineering design considerations, including beam shutter systems, filter structures, and irradiation room layout, as well as experimental validation of the simulated beam parameters.

Conflict of Interest

The authors declare no potential conflict of interest regarding the publication of this work.

Funding

The authors declare that no funds, grants, or other financial support were received during the preparation of this manuscript.

References

Aswal, D. K., Sarkar, P. S., and Kashyap, Y. S. (2022). *Neutron imaging: basics, techniques and applications*. Springer.

Bagheri, R., Afarideh, H., Ghannadi-Maragheh, M., et al. (2015). Production of ^{223}Ra from ^{226}Ra in tehran research reactor for treatment of bone metastases. *Journal of Radioanalytical and Nuclear Chemistry*, 304(3):1185–1191.

Bavarnegin, E., Jafarzadeh, M., Gholamzadeh, Z., et al. (2025). Redesign, construction and commissioning of a powder neutron diffractometer in Tehran research reactor. *Annals of Nuclear Energy*, 213:111055.

Dastjerdi, M. C., Khalafi, H., Kasesaz, Y., et al. (2016a). Design, construction and characterization of a new neutron beam for neutron radiography at the Tehran Research Reactor. *Nuclear Instruments and Methods in Physics Research Section A: Accelerators, Spectrometers, Detectors and Associated Equipment*, 818:1–8.

Dastjerdi, M. H. C., Khalafi, H., Kasesaz, Y., et al. (2016b). Inspection of domestic nuclear fuel rods using neutron radiography at the Tehran Research Reactor. *Materials Testing*, 58(9):763–766.

Dastjerdi, M. H. C. and Khalafi, H. J. P. (2015). Design of a thermal neutron beam for a new neutron imaging facility at tehran research reactor. *Nuclear Engineering and Design*, 69:92–95.

Forughi, S., Hamidi, S., Khalafi, H., et al. (2013). Production of medical radioisotope ^{153}Sm in the tehran research reactor (trr) through theoretical calculations and practical tests. *Annals of Nuclear Energy*, 57:16–21.

Hashimoto, T. (2022). *Principles and applications of X-ray, light and neutron scattering*. Springer.

Joseph, B., Nicolet, M. J. E. J. O. R., and Medicine, N. (2025). A systematic review on neutron radiography: applications, advantages, and challenges. *Journal of Neutron Research*, 56(1):119.

Kasesaz, Y., Bavarnegin, E., Golshanian, M., et al. (2016). BNCT project at Tehran Research Reactor: current and prospective plans. *Progress in Nuclear Energy*, 91:107–115.

Kasesaz, Y., Khalafi, H., Rahmani, F., et al. (2014). Design and construction of a thermal neutron beam for BNCT at Tehran Research Reactor. *Applied Radiation and Isotopes*, 94:149–151.

Lehmann, E. H. (2009). Neutron imaging methods and applications. In *Neutron Applications in Earth, Energy and Environmental Sciences*, pages 319–348. Springer.

Mokhtari, J. and Dastjerdi, M. C. (2023). Development and characterization of a large thermal neutron beam for neutron radiography at Isfahan MNSR. *Nuclear Instruments and Methods in Physics Research Section A: Accelerators, Spectrometers, Detectors and Associated Equipment*, 1051:168209.

Mühlbauer, M. J. et al. (2005). Development of a system for neutron radiography and tomography. *Neutron Radiography and Tomography*, 542(1-3):324–328.

Nallaperumal, M., Namboodiri, G. N., and Roy, T. (2022). Neutron imaging for aerospace applications. In *Neutron Imaging: Basics, Techniques and Applications*, pages 237–252. Springer.

Roy, T. (2022). Basic principles of neutron radiography and tomography. In *Neutron Imaging: Basics, Techniques and Applications*, pages 163–180. Springer.

Tawalare, P. K. (2022). Borate phosphors for neutron radiography. In *Borate Phosphors*, pages 277–301. CRC Press.

Vosoughi, S., Rovias, M. R. A., Rahiminezhad, A., et al. (2023). Production assessment of ^{195m}Pt in Tehran research reactor. *Journal of Radioanalytical and Nuclear Chemistry*, 332(8):2989–2994.

Waters, L. S. and Laboratory, L. A. N. (2002). *MCNPX user's manual*. Los Alamos National Laboratory (LANL).

To cite this article:

S. Sabouri, Y. Kasesaz, M. Kheradmand Saadi. Design of neutron beam for neutron radiography base on the use of TRR thermal column. *Radiation Physics and Engineering*, In Press.

DOI:

To link to this article: